High-Frequency Differential Piezoelectric Photoacoustic Investigation of Ion-Implanted (100) Silicon Wafers via Laser Beam Position Modulation

JOHNNY F. ZUCCON AND ANDREAS MANDELIS, MEMBER, IEEE

***Abstract*—An exploratory application of a new technique, position modulation photoacoustic imaging of ion-implanted (100)-oriented Si wafers was undertaken to assess its potential as a diagnostic probe in semiconductor processing. Wafer scans were performed using acousto-optic modulation of a 1.06 µm Nd^{3+} : YAG laser beam up to 0.2 MHz with piezoelectric photoacoustic detection. Sensitivity ranges to ion-implanted parameters (ionic species and fluences) were studied and the capability of the technique to monitor processing-induced damage was established. Results indicate that position-modulated photoacoustic detection offers higher sensitivity than single-beam photothermal imaging and has distinct advantages over other analytical techniques such as RBS.**

I. Introduction

THERMAL WAVE physics [1], [2] has recently emerged as an important analytical and diagnostic tool in the semiconductor technology [3]–[5]. The ability of thermal waves to perform nondestructive studies in semiconducting materials and processed device chips has been recognized and exploited for some time [5]–[10]. In early communications, Coufal and Pacansky [11], [12] discussed several methods for increasing the resolution and sensitivity of photoacoustic (PAS) techniques. These authors suggested an enhancement in depth resolution obtained from a differential technique utilizing two separate gas microphone PAS cells, a common light source and a beamsplitter. This scheme was expected to result in submicron depth resolution from well-defined subsurface thicknesses inside the material under investigation. In an attempt to monitor semiconductor processing parameters, conventional microphone–gas coupled PAS has been used in the study of Si^{+} implants in GaAs [13], [14] and has demonstrated its capability to detect damage layers resulting from ion implantation. Results from work in laser annealing applications [6], [15] have further demonstrated that microphone–gas coupled PAS can be used to detect variations in semiconductor crystallinity. These previous studies used microphone–gas coupled photoacoustic detection because of the high sensitivity of microphones and/or the commercial availability of PAS cells, however, constraints on the frequency response (transfer function) of microphone transducers have imposed severe limitations on the depth resolution capabilities of these techniques [16]. Specifically, the low-frequency (< 10 kHz) roll-off of the transfer function of commercially available microphones tends to limit the depth resolution of thermal waves in crystalline semiconductors to thicknesses on the order of 20–30 μm, while most microelectronic device active regions lie in submicron ranges. With the advent of piezoelectric detection photoacoustic techniques [17], [18], the study of shallow layers has become feasible.

In this paper a new differential photoacoustic laser beam method is presented, which is a high-speed modification of the methods used by Coufal and Pacansky [11], [12]. The technique relies on an acousto-optically diffracted (i.e., position-modulated) Nd^{3+}–YAG optical beam being used both as a probe and reference for piezoelectric PAS detection. The sensitivity of the technique to ion-implant parameters is demonstrated for a wide range of implant fluences and energies on silicon wafers. Differential mode photoacoustic experiments have been reported previously: To name a few, Lahmann *et al.* [19] used a dual-wavelength technique to increase the spectroscopic sensitivity of PAS to the identification of small amounts of nonfluorescent absorbers in liquids; Hoshimiya [20] also took advantage of differential absorption at different optical wavelengths to enhance the PAS signal-to-noise ratio (SNR) in condensed phases; and very recently Quimby [21] introduced a position-swept real-time PAS technique to map defects in solids with a somewhat poorer SNR than conventional photoacoustic microscopy (PAM). The present work has resulted in the first reported high-frequency, semiconductor parameter sensitivity study of differential piezoelectric photoacoustic detection applied to ion-implanted silicon, and a direct comparison with sin-

Manuscript received May 1, 1986; revised January 23, 1987; accepted January 23, 1987. This work supported by a Strategic Grant of the National Sciences and Engineering Research Council of Canada.

J. Zuccon is with the Optical Recording Corporation, 141 John St., Toronto, ON, Canada M5V 2E4.

A. Mandelis is with the Department of Mechanical Engineering, University of Toronto, 5 Kings's College Rd., Toronto, ON, Canada M5S 1A4.

IEEE Log Number 8717127.

0885-3010/88/0100-0005$01.00 © 1988 IEEE

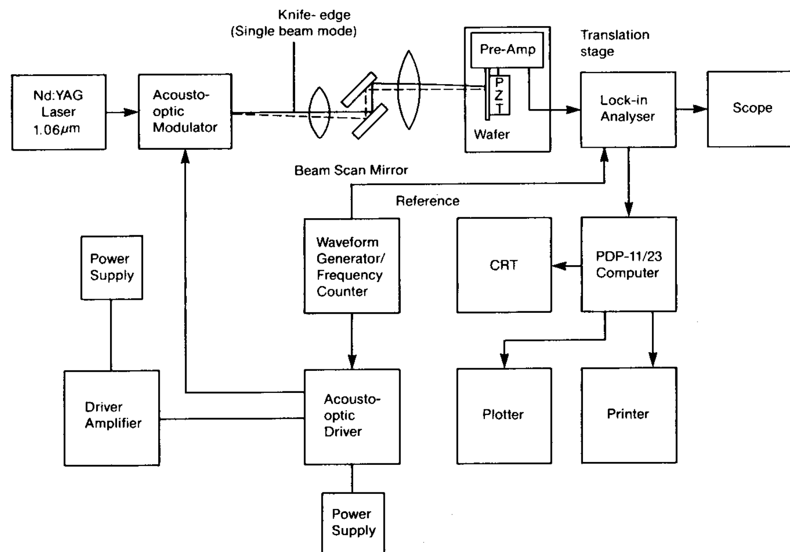

Fig. 1. Experimental apparatus for differential and single-beam piezoelectric photoacoustic detection.

gle-beam detection. Previously, Ringermacher *et al.* [22], [23] have described a similar coordinate modulation technique for the case of electron-acoustic imaging of solid materials.

II. Instrumentation and Materials

Fig. 1 shows the PAS experimental apparatus used to perform both differential and single-beam studies on silicon wafers. A General Photonics Two-15 CW Nd^{3+}-YAG laser emitting approximately 2W of optical power at 1.06 μm was used in series with an Isomet 1201 acousto-optic modulator. A knife-edge was inserted in the optical circuit only when single-beam studies were desirable. Samples were pressed in intimate contact with a homemade piezoelectric detector unit upon using silicone as the interface, for nondestructive photoacoustic studies. The detector unit consisted of a lead-zirconate-titanate (PZT) piezoelectric ceramic (Vernitron PZT-5H) with a resonant frequency of 0.2 MHz. The transducer was confined in a stainless steel housing with a removable back plate. The front end of the transducer was in acoustic contact (via a thin layer of vacuum grease) with the cap of the housing (diaphragm), which consisted of an approximately 500-μm-thick stainless steel shim cold soldered onto the stainless steel chassis. To increase the reflectivity, and thus minimize any synchronous signals originating at the transducer cage, a thin (50 Å) gold layer was vacuum sputtered on the diaphragm surface. The transducer assembly is shown schematically in Fig. 2. The overall design is similar to one used previously for solid [18] and liquid phase [24] PAS studies. An additional merit of the detector housing design was the effective shielding of the PZT transducer it provided against electromagnetic interference from the environment, acting as a Faraday cage. A translational stage, on which rested the

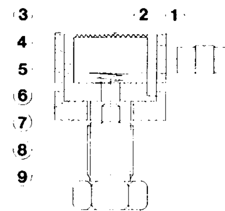

Fig. 2. Cross-sectional view of spring-loaded PZT detector cage: 1) BNC connector; 2) acoustic coupling medium (vacuum grease); 3) diaphragm (Au-coated stainless-steel shim); 4) PZT-5H piezoelectric transducer (top face: ground; bottom face: high lead to BNC); 5) spring-loaded electrode; 6) stainless-steel housing chassis; 7) PZT retainer support (Plexiglas); 8) housing back plate; 9) pressure-adjusting screw.

sample holder and the preamplifier (Ithaco model 1201 low-noise pre-amplifier with adjustable gain control) was fabricated allowing laser beam scanning in two dimensions on a fixed plane perpendicular to the direction of the beam propagation. The amplified signals were fed into either a low-frequency lock-in analyzer (EG&G Model 5204) or a high-frequency one (EG&G Model 5202), depending on the frequency of the photoacoustic scan. The appropriate lock-in analyzer was coupled to a fast 12-bit Data Translation A/D converter Model DT 3392, used to transfer data for storage on hard disk through a Digital Equipment RL02 disk drive. The entire apparatus was mounted on a Newport Corp. optical table to achieve maximum vibrational isolation.

Materials used in these studies included: a) unprocessed (100)-oriented 4-in-diameter Si wafers for testing the apparatus; b) processed 4-in-diameter Si wafers with a step-like interface between a 0.355-μm-thick layer of polycrystalline silicon and a 1.0-μm-thick SiO_2 field oxide thermally grown layer; and c) a matrix of 4-in-diameter (100)-oriented Si wafers, ion-implanted in half surface area at Northern Telecom Electronics, Ottawa,

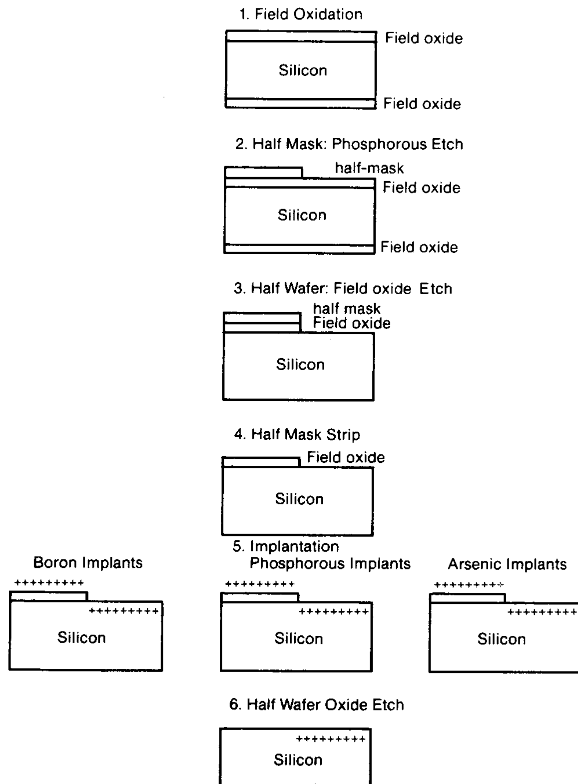

Fig. 3. Process flow chart for ion-implanted 4-in-diameter, (100)-oriented Si wafers.

Canada, with a range of doses of B^+, P^+ and As^+ ions typical of industrial applications. The implant energies used were 50, 100 and 150 keV with fluence levels ranging from 10^{12} to 10^{16} ions/cm^2, representing characteristic parameters for microelectronic device processing. A process flow chart of the implanted wafer matrix is shown in Fig. 3.

III. Technique Characterization and Experimental

Single laser beam photoacoustic scans across sample surfaces of variable features have been previously reported [25]–[27]. Those applications were able to demonstrate the technique's capability for depth profiling, for instance in metal samples with artificially introduced defects in the form of holes drilled into the sample [25], [28]. With thin subsurface damage layers such as those resulting from ion implantation, photoacoustic detection is more complicated. The thin damage layers are usually at shallow depths in the material and therefore require thermal diffusion lengths in the submicron range for complete depth resolution [4]. In silicon this requirement entails high modulation frequencies in the neighborhood of 100 MHz to resolve typical ion-implant profiles of 2000–3000 Å thickness [29], [30]. At very-high-modulation frequencies the piezoelectric PAS SNR, however, is expected to decrease substantially due to the decreased amounts of optical energy imparted to the sample per modulation period [31]. An additional difficulty appears at modulation frequencies beyond 20 MHz due to ultrasonic limitations, since the wavelength of the acoustic carrier wave becomes small enough to introduce acoustic imaging [32], which may complicate the thermal wave information received by the piezoelectric transducer. For most realistic piezoelectric PAS experiments with shallow defect materials, the single-beam technique can provide at best integrated signals comprising information from both the damaged layer and part of, or all of, the substrate. Analytical vectorial methods have been suggested [33] to help isolate amorphous layer signal contributions from the integrated PAS signal. Utilizing optical excitation sources of appropriate wavelengths so as to eliminate substrate bulk absorption (e.g., the Nd^{3+}–YAG 1.32 μm line for scanning Si substrates) has also been suggested [14].

In our experiments we exploited the spatial separation of the first-order diffracted beam emerging from the acousto-optic modulator from the zeroth-order undeflected beam [34]. The zeroth-order beam provided the signal reference and was incident on the crystalline side of the interface dividing the implanted and unimplanted half surfaces of the processed wafers (Fig. 3). The first-order diffracted beam acted as both the exciting and the probe beam, so that the total amount of optical energy was always present on the sample. Higher diffracted orders were present also, however, the amounts of power imparted into those orders were found to be negligible compared to the zeroth and first orders, in qualitative agreement with the theory of acousto-optic light modulation [34]. Focussing of the beam resulted in an increase in the lateral resolution of the scans and allowed for smaller beam separation distances to be used. This feature tended to decrease background signals arising from spatial response nonuniformities of the PZT transducer. Care was taken to divide the input optical power at the 50 percent level between the zeroth and first-order beams, with the lock-in analyzer registering effectively a zero-level A.C. (i.e. a D.C.-level) photoacoustic differential signal from a homogeneous, crystalline Si wafer. Fig. 4 explains the differential technique. The reference signal from the waveform generator to the lock-in is shown in Fig. 4(a). The zeroth-order undiffracted beam is in phase with the square wave reference. The video input to the modulator was a sinewave that resulted in an intensity output proportional to the square of the modulated optical field, i.e., $\cos^2 \omega t$, as shown in Fig. 4(b). The first-order beam intensity modulation is thus phase-shifted by 180° with respect to the reference waveform, Fig. 4(c). The superposition of the zeroth and first-order intensities over time is, therefore, expected to produce approximately (neglecting higher orders) a constant intensity as shown in Fig. 4(d). Thus, our differential technique when employed to scan over a spatially uniform sample is expected to produce a constant amplitude (dc-level) signal with a phase given by the sum

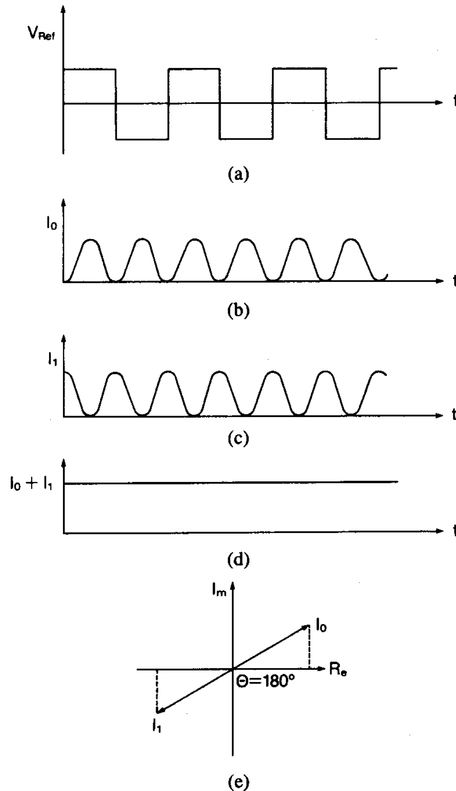

Fig. 4. Mechanism of differential photoacoustic technique. (a) Typical square wave input reference; (b) Zeroth beam intensity modulation wave-form. (c) First-order beam intensity modulation wave-forms. (d) Temporal superposition of two orders. (e) vector (phasor) representation of I_0 and I_1 signals in complex plane.

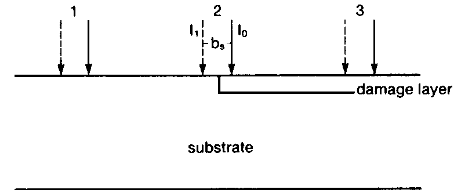

Fig. 5. Schematic illustration of position-modulated differential photoacoustic scan.

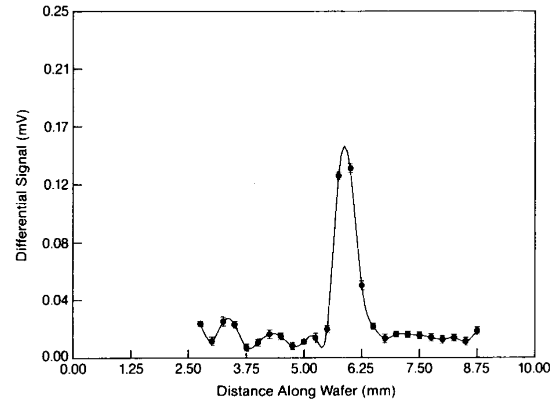

Fig. 6. Position-modulated differential PAS scan at 2 kHz for Si substrate with polysilicon/SiO_2 interface.

of 180° plus material contributions. This feature is indicated in Fig. 4(e).

Experimental results on the differential PAS amplitude and phase from a 20 kHz scan across the interface between a SiO_2 and polysilicon layer on Si substrate confirmed the above considerations: the amplitude was essentially spatially constant and low when either side of the interface was scanned and rose to a higher level when the two beams straddled the interface. The phase exhibited a small variation about 180° in the position of the interface, otherwise was essentially flat throughout the entire scan. Fig. 5 shows a schematic representation of the position-modulated experiments. When the two beams of approximately equal optical power scanned the same or similar materials, positions 1 and 3 in Fig. 5, the differential photoacoustic signal was low and spatially constant (with the notable exception of the polysilicon surface). When the two beams straddled the interface between materials of different thermal and optical properties a strong and spatially variable differential photoacoustic signal was recorded. A differential beam scan across the same polysilicon and SiO_2 region performed at 2 kHz is shown in Fig. 6 to demonstrate the nature and levels of signals involved in a typical process of the type illustrated in Fig. 5.

The frequency response characteristics of the transducer cage assembly when irradiated directly with position-modulated light in a differential mode are shown in Fig. 7(a). The results from a single-beam frequency scan are shown in Fig. 7(b) for comparison. The broad frequency response of thc PZT-5H offers good SNR in both the low (<3 kHz) and high (>50 kHz) ranges, especially at or near the transducer's resonant frequency (≈ 200 kHz). It is interesting to note that, while both techniques bear out the expected signal frequency dependence [28], [31], [35], at low frequencies, the differential technique exhibits stronger signal levels throughout the midrange frequencies. A direct numerical comparison of absolute signal values between the single-beam and differential technique was not feasible, since they have different reference levels. The nonzero ac signal shown in Fig. 7(a) is unexpected in view of the mechanism put forth in Fig. 4, however, it can be explained in terms of spatial inhomogeneities of the transducer response. These inhomogeneities constituted the single most important drawback of our technique in a global sense, as they required the mapping and normalizing out of the photoacoustic response of the transducer in all subsequent scans. With our Vernitron transducer, we were not able to confirm previous findings of PAS signal enhancement upon application of a square wave input to the acousto-optic modulator, compared to a sinusoidal wave [17]; the signal levels we obtained from both types of input wave-forms were essentially identical.

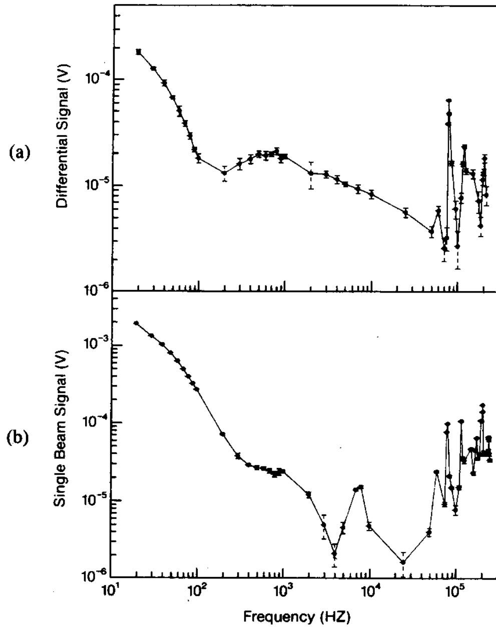

Fig. 7. Frequency response of PZT-5H transducer cage. (a) Differential mode; (b) Single-beam method.

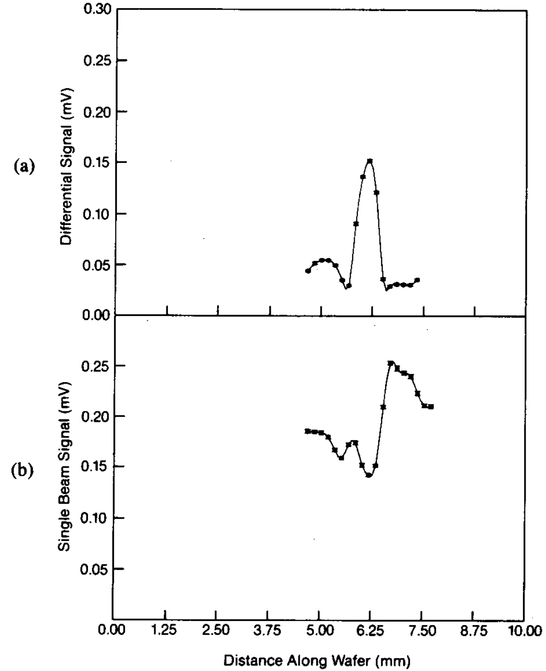

Fig. 8. PAS amplitude from scans of P^+-implanted Si (150 keV, 10^{16} ions/cm^2) across interface. (a) Position-modulated differential scan. (b) Single-beam method.

A matrix of ion-implanted silicon wafers was also used to evaluate the sensitivity limits of our technique with respect to the detection of low- and high-level damage resulting from the implantation process. Both position-modulated differential and single-beam scans were performed. To maximize the reproducibility of our technique, only single line scans were recorded; in this mode any signal contribution from the direct response of the transducer itself was found to be minimal. Wafer scans covering approximately a 3-mm range and centered at the implanted/crystalline interface were performed. The modulation frequency was 0.2 MHz (at the PZT resonance peak) with a zeroth-to-first-order beam separation of approximately 0.5 mm and a scan increment step of 0.17 mm. The beam separation at the sample surface could be controlled through adjustment of the focussing lenses of the beam scan mirror assembly (Fig. 1). The beam spotsizes were approx. 50 μm at the sample. Strong differential PAS signals were obtained from scanning through the interfacial features of the ion-implanted wafers of Fig. 3. For purposes of comparison the samples were scanned using both single beam and differential methods. Fig. 8 is representative of a typical scan result. The differential PAS response is characteristic of local variations in the optical and thermal environment on either side of the interface. The corresponding single beam PAS response produced a step-like discontinuity, as expected. These results show that the position-modulation method smoothens out background signals induced by inhomogeneities in thermal and/or optical properties of neighboring implanted sites, in addition to transducer-related background signals.

The smooth low level differential signal from the unimplanted side of (C) right of the peak, Fig. 8(a), is expected and should be compared to the widely varying single-beam signals from the same location, Fig. 8(b). The implanted region of (B) left of the peak in Fig. 8(a) produced scan signals with pronounced irregularity as expected, due to local variations in the degree of damage incurred in the crystal lattice by the ion implanter. This effect, although also present in Fig. 8(b), is difficult to assess with the single-beam scan because of the inherent superposition of the background nonuniformity. From the ratio of the differential peak signal (A) in Fig. 8(a) to the average crystalline Si signal (C), a fourfold signal increase at the interface could be observed. The contrast is much poorer in the single-beam results ($(A)/(C) \approx 1.1$ in Fig. 8(b)). Similarly on the implanted side the ratio $(A)/(B)$ is 3 and 1.5, respectively.

IV. Results and Discussion

The peak differential signals obtained from 200 kHz scans of 150 keV P^+ implanted Si wafers are shown in Fig. 9. This figure is indicative of the sensitivity of position modulation PAS to fluence levels as low as 10^{12} ions/cm^2. Unfortunately, no samples implanted with lower fluences were available in these experiments to establish a lower sensitivity limit. The damage density by implantation of a given ion species is expected to increase with increasing ion fluence. Damage saturation at high implant doses was previously observed by McFarlane *et al.* [13], [14], in microphone–gas coupled PAS experiments with Si^+ implanted GaAs. Those authors attributed saturated PAS signals approximately above 10^{14} ions/cm^2

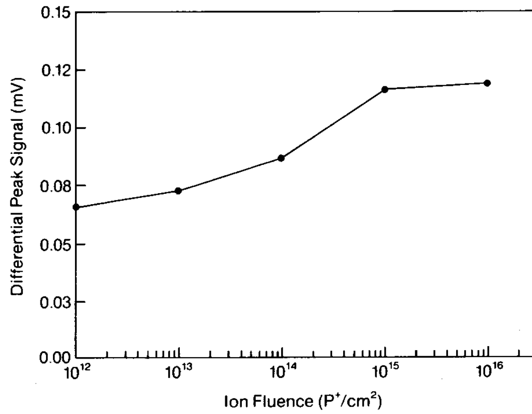

Fig. 9. Differential peak PAS signal amplitudes from P^+-implanted Si wafers at 150 keV. Standard deviations are smaller than the size of experimental points.

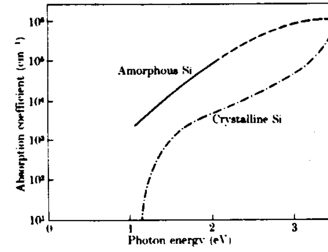

Fig. 10. Optical absorption edges in evaporated and crystalline silicon (after [36]).

to complete amorphization of the implanted region. A similar trend is evident in Fig. 9 for doses on the order of 10^{15} ions/cm^2. The increasing PAS signal with higher ion fluence can be attributed to changes in the optical and thermal properties of the implanted region due to an increased damage density. At 1.06-μm irradiation, the incident photon energy (E_p = 1.17 eV) is slightly above the bandgap energy of silicon (E_g = 1.12 eV at 300°K) [36]. Crystalline silicon is, therefore, semitransparent at 1.06 μm (optical absorption coefficient $\beta_{Si} \approx 10$ cm^{-1} [37]). Amorphous thin films of silicon have been found to have absorption coefficients on the order of 5×10^3 cm^{-1} in the 1.1–1.2 eV spectral region [38], Fig. 10. Assuming that amorphous or quasi-amorphous layers produced by ion implantation may not be too different optically from thin films glow-discharge deposited, sputtered or evaporated on substrates [38], the major cause of the increased PAS signal with increased ion fluence may be taken to be the increase of β_{Si} upon the onset and increase in the degree of amorphization. Similar increases of PAS signals due to subbandgap defects in a-Si : H ion-beam deposited films have been previously observed [39] and attributed to changes in the optical absorption coefficient below the bandgap. Other sources of the differential peak signals observed in Fig. 9 may include the poorer thermal properties of the implanted layer and changes in the reflectivity of this layer [6]. These interpretations are also supported by piezoelectric photoacoustic experiments performed by Jackson and Amer [31]. These authors concluded that strongly absorbing samples retain more heat and thus produce larger material strains.

Recently, Smith *et al.* [40], [41], utilized the technique of sample reflectivity modulation with temperature as monitored via the intensity changes of the reflected beam of a tightly focussed probe He–Ne laser from Si wafer surfaces. The temperature modulation resulted from an intensity modulated heating Ar^+ laser [42]. These authors performed ion implantation studies using 50 keV B^+ ions with fluences between 10^{11} cm^{-2} and 10^{15} cm^{-2}. Although no direct comparison can be made with Fig. 9 of this work due to the different ion species and detection principle, the trends in the data from both sets of investigations are similar: The ability of their technique to monitor ion implants at fluences below 10^{12} cm^{-2} is consistent with our findings. In Fig. 9 we demonstrated that fluence monitoring up to 10^{16} cm^{-2} of P^+ implants is possible without signal saturation, in agreement with the nonsaturated character of the data by Smith *et al.* (Fig. 1, [40]) up to 10^{15} B^+/cm^2. The PAS signal variation of approximately 5 units (i.e. mV) from the baseline in Fig. 9 between 10^{12} and 10^{16} P^+/cm^2 fluences is certainly comparable to the difference of 9 thermal wave units for the same span of B^+ fluences in Fig. 1, [40]. It thus appears that our technique gives comparable results to the experimentally more complicated (and expensive) reflectivity modulation method of Smith *et al.* An increased degree in sensitivity of the method by Smith *et al.* may be attributed to the partly transparent nature of the Si wafers at 1.06 μm, compared to the opacity of Si at the 488 nm line of the Ar^+ laser used by those authors. Large synchronous signals generated due to the spatial inhomogeneity of the transducer response during scanning across its surface had to be normalized out in obtaining the results of Fig. 9. For this reason, the sensitivity of our technique, measured by the difference between signal maximum and minimum response in Fig. 9 is

$$[(S_{max} - S_{min})/S_{max}] \times 100 = \text{approx 70 percent},$$

lower than that obtained by Smith *et al.* [40] (= approx 200 percent for the same fluence range of B^+ implant). It appears that a disadvantage of using a PZT transducer in the scanning mode is the degree of response inhomogeneity across its surface, which requires painstaking normalization of the photoacoustic signal. The method by Smith *et al.*, however, has the added advantage of truly noncontact Si lattice damage monitoring, thus eliminating all probability of wafer contamination due to the transducer bonding medium present in this work.

McFarlane *et al.* [14] used a single-beam photoacoustic scan to map the damage induced in Si ion-implanted with 220 keV As^+ with fluences between 2×10^{15} and 1×10^{16} ions/cm^2. They operated a CW Nd^{3+} : YAG laser at 1.32 μm in order to avoid substrate absorption effects at 1.06-μm excitation. Similar effects were, in principle,

present in our experiments, however, the differential scanning method employed in this work automatically subtracts out substrate absorption related background signals, thus giving PAS signals primarily from the thin implanted layers. This useful feature minimizes the need to use extremely high frequencies (> 100 MHz) in order to isolate photoacoustic effects from the thin implanted films [4] and minimizes substrate contributions to the signal.

The results from Si^+ implanted GaAs reported by McFarlane *et al.* [13], [14], show that sensitivity to implantation damage of the microphone-gas coupled PAS system at low modulation frequencies was limited to doses greater than 10^{12} ions/cm^2. When compared with the minimum signal level of Fig. 9, it becomes apparent that our differential technique is capable of detecting even lower fluences than 10^{12} ions/cm^2, a task that is quite difficult for Rutherford back scattering (RBS) analysis. At the high-fluence level end of ion implantation, the experiments by McFarlane *et al.* indicate complete saturation and, perhaps, the onset of a self-annealing effect in the 10^{16} ions/cm^2 range. The plot of Fig. 9 shows that the high-frequency differential signal is not yet fully saturated in the same fluence range. This effect could be due to the high frequencies employed in our experiments keeping the PAS signal out of photoacoustic saturation [43], as expected from a thermally thick, optically opaque geometry. Unfortunately, no numerical verification of this claim is possible at this time, as the thermal diffusivity of the implanted layers is unknown.

Fig. 11 shows differential PAS amplitude data of the signal at the interface as a function of ion-implant species. The curves labeled (A), (B) and (C) correspond respectively to 1) the peak differential signal at the interface, the average signal level on the implanted side; and the average signal level form the unimplanted side. These results were plotted against atomic mass number of the ion species. The trends illustrated in Fig. 11 can be qualitatively understood as follows: The increase in atomic mass of the implant species decreases the effective penetration depth in the material, as indicated by the projected range statistics of the Lindhard, Scharff and Schlott (LSS) theory [44]. According to the Rosencwaig-Gersho (RG) theory [43], the PAS signal in optically transparent solids is expected to decrease with βl, where l is the effective thickness of the implanted layer in this case, and β is the absorption coefficient of this layer. Therefore, a decrease in PAS signal level with increasing atomic mass is expected, since the heavier ions will penetrate less into the lattice, thus decreasing l. This will be so, provided β changes of the damaged layer with ion species do not dominate the βl product. Curves (A) and (B) in Fig. 11 bear out these expectations, with the exception of curve (B) in Fig. 11(c). It is further expected that the unimplanted silicon side should possess the largest degree of material uniformity, and thus the PAS signal must be essentially independent of ion size. This is indeed the case, as presented by curves (C) in Fig. 11, in which the average crystalline Si signal is shown to be the least sensitive to ion species variation. The lack of absolutely constant levels has been attributed to deviations due to the number of samples taken to calculate the averages of Fig. 11. A similar tentative explanation has been advanced regarding the anomaly of curve (B) in Fig. 11(c), in view of the relatively weak signal averaging involved in the 50-keV case.

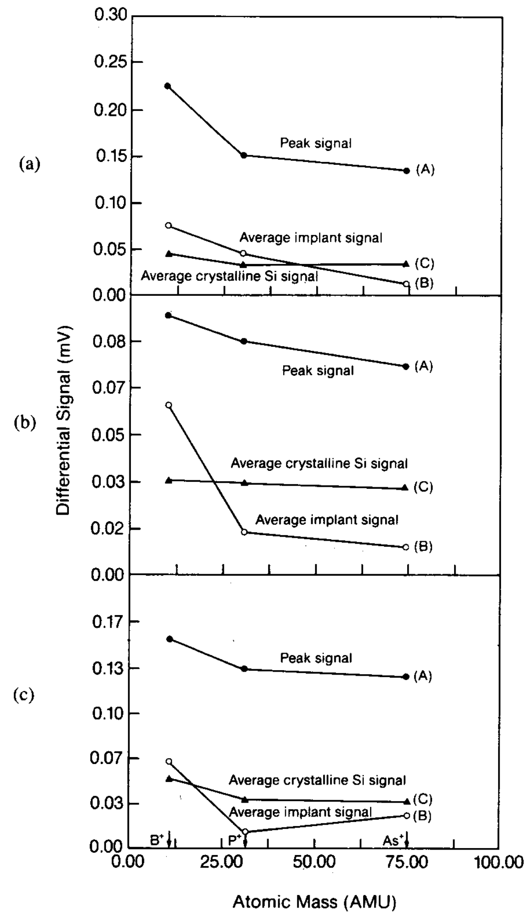

Fig. 11. Differential PAS signal amplitudes as function of ion implant species. (a) 150 keV, 1×10^{16} ions/cm^2. (b) 100 keV, 1×10^{14} ions/cm^2. (c) 50 keV, 1×10^{12} ions/cm^2. The letters A, B, C correspond to peak, implanted, and unimplemented regime of Fig. 8(a), respectively. Standard deviations are of same magnitude as point size.

An attempt to assess the effects of ion-implant damage on the optical properties of the Si wafers was made by acoustically isolating the wafers from the PZT transducer diaphragm surface with 2-mm spacers. The acoustic signal produced from direct light transmission through the wafer was monitored for both the processed and unimplanted sides of the interface. The amount of light transmitted through the implanted side was found to be less than that transmitted through the crystalline side that was almost entirely transparent to the 1.06-μm radiation. An average decrease in signal levels of approximately 38 percent was found for a 150-keV As^+ implanted wafer. Light scattering through the damaged layer and the concommi-

TABLE I
IMPLANT-ION ENERGY EFFECTS ON PAS DIFFERENTIAL SIGNALS

A Ion Species	B Fluence (ions/cm^2)	C Energy (keV)	D Ratio*
P^+	10^{14}	150	0.85
P^+	10^{14}	100	0.47
P^+	10^{12}	150	0.78
P^+	10^{12}	50	0.34

*Ratio ≡ [Average implanted signal (B)]/[Average unimplanted signal (C)]; B, C as in Fig. 8(a).

tant reflectivity changes would tend to alter the transmitted fraction, however, no attempt was made to assess their effect separately in this work. The anticorrelation observed between transmission acoustic and PAS piezoelectric signals of the implanted layers with respect to the unimplanted Si, further corroborates that the piezoelectric signals measured with the wafers in place were due to the photoacoustic effect in the materials, rather than due to synchronous acoustic waves resulting from direct light transmission to the transducer diaphragm.

Even though the degree of amorphization of the implanted layers of our wafer matrix was not known, these layers did behave photoacoustically like amorphous or quasi-amorphous thin films, producing an increased PAS signal with increasing implantation energies, consistently with previous observations [6] on PAS signal dependence on the degree of silicon crystallinity. Table I shows typical results of P^+-implanted wafers. The ratio in column D is used so as to remove any discrepancies due to the effect of variable contact pressure with the transducer from sample to sample.

The usefulness of photoacoustic phase imaging has been reported by various authors [16], [25], [26], [35], claiming an increase in depth sensitivity over PAS amplitude information. Busse and Rosencwaig [25] showed that phase detection results in a depth sensitivity of $1.5 \times$ the thermal diffusion length [43] in gas-coupled microphone cells and an even greater one ($>2\times$) with piezoelectric detection. The published work with photoacoustic phase results has been essentially restricted to metal and metal void investigations [26], [45]. In the present work phase information from the ion-implanted wafers was less generous and much more irregular than those previous studies. Our differential technique may be too sensitive for differential phase imaging. The phase results from scans of the ion-implanted wafers were thus not included in the discussion.

V. CONCLUSION

A frequency-domain differential piezoelectric photoacoustic investigation of ion-implanted (100) Si wafers has been carried out in order to assess the usefulness of this technique as an implant damage probe. The results showed that the sensitivity (at least in terms of signal-to-noise ratio) of the position-modulated photoacoustic signal across the implantation interface is superior to that obtained with a single modulated beam scanned across the interface. The new technique was found to be sensitive to a broad range of implant species (B^+, P^+, and As^+) and ion fluences ($< 10^{12}$ cm^{-2} and $> 10^{16}$ cm^{-2}).

ACKNOWLEDGMENT

The authors wish to thank Dr. H. Naguib of Northern Telecom Electronics, Advanced Processing Silicon R&D Department, Ottawa, for supplying the ion-implanted wafers.

REFERENCES

[1] A. Mandelis, "Hamilton-Jacobi formulation and quantum theory of thermal wave propagation in the solid state," *J. Math. Phys.*, vol. 26, pp. 2676–2683, 1985.

[2] F. A. McDonald, "Photoacoustic effect and the physics of waves," *Am. J. Phys.*, vol. 48, pp. 41–47, 1980.

[3] A. Rosencwaig and R. M. White, "Imaging of dopant regions in silicon with thermal-wave electron microscopy," *Appl. Phys. Lett.*, vol. 38, pp. 165–167, 1981.

[4] A. Rosencwaig, "Thermal-wave microscopy," *Solid State Technol.*, vol. 25, pp. 91–97, Mar. 1982.

[5] —, "Nondestructive evaluation with thermal waves," *J. Photoacoust.*, vol. 1, pp. 371–386, 1983.

[6] J. F. McClelland and R. N. Kniseley, "Photoacoustic signal changes associated with variations in semiconductor crystallinity," *Appl. Phys. Lett.*, vol. 35, pp. 585–587, 1979.

[7] L. D. Favro, P. K. Kuo, J. J. Pouch, and R. L. Thomas, "Photoacoustic microscopy of an integrated circuit," *Appl. Phys. Lett.*, vol. 36, pp. 953–954, 1980.

[8] J. Opsal and A. Rosencwaig, "Thermal-wave depth profiling: Theory," *J. Appl. Phys.*, vol. 53, pp. 4240–4246, 1982.

[9] M. Kasai, T. Sawada, and Y. Gohshi, "Photoacoustic microscopic (PAM) images of some GaAs wafers," *Jpn. J. Appl. Phys.*, vol. 24, Suppl. 24-1, pp. 220–221, 1985.

[10] M. Kasai, H. Shimizu, T. Sawada, and Y. Gohshi, "Non-destructive observation of stacking faults of silicon wafers by means of photoacoustic microscopy," *Anal. Sci.*, vol. 1, pp. 107–109, 1985.

[11] H. Coufal and J. Pacansky, "High resolution photoacoustic spectroscopy," *IBM Tech. Discl. Bull.*, vol. 22, pp. 4681–4683, 1980.

[12] —, "Differential photoacoustic analysis of semiconductors," *IBM Tech. Discl. Bull.*, vol. 23, pp. 3861–3862, 1981.

[13] R. A. McFarlane and L. D. Hess, "Photoacoustic measurements of ion-implanted and laser-annealed GaAs," *Appl. Phys. Lett.*, vol. 36, pp. 137–139, 1980.

[14] R. A. McFarlane, L. D. Hess, and G. L. Olson, "Two-dimensional photoacoustic mapping of ion-implanted and laser annealed semiconductors," *IEEE Ultrason. Symp.*, pp. 628–632, 1980.

[15] J. F. McClelland and R. N. Kniseley, "Photoacoustic characterization of CW argonion laser irradiation of Ge," *Appl. Phys. Lett.*, vol. 35, pp. 121–124, 1979.

[16] A. Rosencwaig and G. Busse, "High-resolution photoacoustic thermal-wave microscopy," *Appl. Phys. Lett.*, vol. 36, pp. 725–727, 1980.

[17] M. M. Farrow, R. K. Burnham, M. Auzanneau, S. L. Olsen, N. Purdie, and E. M. Eyring, "Piezoelectric detection of photoacoustic signals," *Appl. Opt.*, vol. 17, pp. 1093–1098, 1978.

[18] A. C. Tam, "Optoacoustic determination of photocarrier generation efficiencies of dye films," *Appl. Phys. Lett.*, vol. 37, pp. 978–981, 1980.

[19] W. Lahman, H. J. Ludewig, and H. Welling, "Opto-acoustic trace analysis in liquids with the frequency-modulated beam of an argon ion laser," *Anal. Chem.*, vol. 49, pp. 549–551, 1977.

[20] T. Hoshimiya, "On the differential absorption photoacoustic spectroscopy," *Jpn. J. Appl. Phys.*, vol. 22, p. 203, 1983.

[21] R. S. Quimby, "Real-time photoacoustic microscopy," *Appl. Phys. Lett.*, vol. 45, pp. 1037–1039, 1984.

[22] H. I. Ringermacher, "Coordinate modulation with piezoelectric detection," *IEEE Ultrason. Symp.*, IEEE Cat. #82CH1823-4, vol. 2, p. 576, 1982.

[23] H. I. Ringermacher and L. Jackman, "Deep thermoacoustic imaging using scanning electron acoustic microscopy," *Rev. Progress in Quantitative NDE*, vol. 5A, p. 567, 1986.
[24] A. C. Tam and C. K. N. Patel, "Optical absorptions of light and heavy water by laser optoacoustic spectroscopy," *Appl. Opt.*, vol. 18, pp. 3348-3358, 1979.
[25] G. Busse and A. Rosencwaig, "Subsurface imaging with photoacoustics," *Appl. Phys. Lett.*, vol. 36, pp. 815-816, 1980.
[26] G. Busse, "Optoacoustic phase angle measurement for probing a metal," *Appl. Phys. Lett.*, vol. 35, pp. 759-760, 1979.
[27] Y. H. Wong, R. L. Thomas, and J. J. Pouch, "Subsurface structures of solids by scanning photoacoustic microscopy," *Appl. Phys. Lett.*, vol. 35, pp. 368-369, 1979.
[28] T. Sawada, H. Shimizu, and S. Oda, "Observation of Subsurface Structures by Scanning Laser Photoacoustic Spectroscopy," *Jpn. J. Appl. Phys.*, vol. 20, pp. L25-L27, 1981.
[29] B. Smith, *Range Data for Silicon and Germanium Device Technologies*. Oxford: Learned Information, 1977.
[30] J. P. Biersack, *Ion Implantation*, H. Ryssel and J. Ruge, Eds. Stuttgart: Teubner, 1978.
[31] W. Jackson and N. M. Amer., "Piezoelectric photoacoustic detection: Theory and experiment," *J. Appl. Phys.*, vol. 51, pp. 3343-3353, 1980.
[32] H. K. Wickramasinghe, R. C. Bray, V. Jipson, C. F. Quate, and R. J. Salcedo, "Photoacoustics on a microscopic scale," *Appl. Phys. Lett.*, vol. 33, pp. 923-925, 1978.
[33] J. F. McClelland, "Condensed Matter Photoacoustic Spectroscopy and Detection using Gas Phase Signal Generation," *IEEE Ultrason. Symp.*, pp. 610-617, 1980.
[34] N. Uchida and N. Niizeki, "Acoustooptic Deflection Materials and Techniques," in *Proc. IEEE*, vol. 61, pp. 1073-1092, 1973.
[35] A. Hordvik and H. Schlossberg, "Photoacoustic technique for determining optical absorption coefficients in solids," *Appl. Opt.*, vol. 16, pp. 101-107, 1977.
[36] S. M. Sze, *Physics of Semiconductor Devices*. New York: Wiley, 1969, p. 20.
[37] W. C. Dash and R. Newman, "Intrinsic optical absorption in single-crystal germanium and silicon at 77°K and 300°K," *Phys. Rev.*, vol. 99, pp. 1151-1157, 1955.
[38] N. F. Mott and E. A. Davis, *Electronic Processes in Non-Crystalline Materials*. Oxford: Clarendon Press, 1979, 2nd Ed. ch. 7, pp. 320-407.
[39] G. P. Ceasar, K. Okumura, J. Lin, M. A. Machonkin, and L. Dudek, "Photoacoustic spectroscopy and charge transport of a-Si : H prepared by ion beam deposition," *J. Non-Cryst. Solids*, vols. 59 and 60, pp. 289-292, 1983.
[40] W. L. Smith, A. Rosencwaig, and D. L. Willenborg, "Ion implant monitoring with thermal wave technology," *Appl. Phys. Lett.*, vol. 47, pp. 584-586, 1985.
[41] W. L. Smith, A. Rosencwaig, D. L. Willenborg, J. Opsal, and M. W. Taylor, "Ion implant monitoring with thermal wave technology," *Solid State Technol.*, vol. 29, pp. 85-92, Jan. 1986.
[42] J. Opsal, A. Rosencwaig, and D. L. Willenborg, "Thermal-wave detection and thin-film thickness measurements with laser beam deflection," *Appl. Opt.*, vol. 22, pp. 3169-3176, 1983.
[43] A. Rosencwaig and A. Gersho, "Theory of the photoacoustic effect with solids," *J. Appl. Phys.*, vol. 47, pp. 64-69, 1976.
[44] J. Lindhard, M. Scharff and H. E. Schlott, *Kal Danske Vedenskab. Selskab. Mat. Fys. Medd.*, vol. 33, pp. 14-24, 1963.
[45] R. L. Thomas, J. J. Pouch, Y. H. Wong, L. D. Favro, P. K. Kuo, and A. Rosencwaig, "Subsurface flaw detection in metals by photoacoustic microscopy," *J. Appl. Phys.*, vol. 51, pp. 1152-1156, 1980.

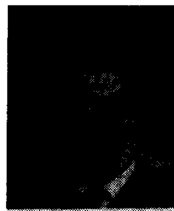

Johnny F. Zuccon was born on March 30, 1960, in Conegliano, Italy. He received the B.A.Sc. degree in mechanical engineering, in 1983 and the M.A.Sc. degree in the photoacoustic and photothermal sciences in 1985 from the University of Toronto, Toronto, ON, Canada.

He has been a Mechanical Design Engineer for the Optical Recording Corp. since November 1985. He is responsible for research and development including analysis of current devices.

Andreas Mandelis (M'86) was born on June 22, 1952, in Corfu, Greece. He received the B.S. degree in physics in 1974 from Yale University. He received the M.A. degree in applied physics in 1976, the M.S.E. degree in mechanical and aerospace engineering in 1977, and the Ph.D. in applied physics in 1979 from Princeton University, Princeton, NJ.

He was a member of the scientific staff (silicon R&D) at Bell Northern Research, Ottawa, ON, Canada, from 1979-1981. He has been an Assistant Professor in the Department of Mechanical Engineering at the University of Toronto, Toronto, ON, Canada, from 1982 to 1986. He is currently an Associate Professor and Director of the Photoacoustic and Photothermal Sciences Laboratory.

Mandelis is a member of the American Physical Society, Sigma Xi, Canadian Association of Physiciests, Spectroscopy Society of Canada, the New York Academy of Sciences, and the ASME.